Unraveling the deposition mechanism in *a*-C:H thin-film growth: A molecular-dynamics study for the reaction behavior of C_3 and C_3H radicals with *a*-C:H surfaces

E. Neyts[a] and A. Bogaerts
Department of Chemistry, University of Antwerp, Research Group PLASMANT, Universiteitsplein 1, 2610 Antwerp, Belgium

M. C. M. van de Sanden
Department of Applied Physics, Eindhoven University of Technology, Den Dolech 2, 5600 MB Eindhoven, The Netherlands

(Received 9 September 2005; accepted 27 October 2005; published online 4 January 2006)

In this molecular-dynamics study, we present the simulated growth of thin *a*-C:H films using the Brenner [(Phys. Rev. B **42**, 9458 (1990)] potential. These simulations are relevant for the growth of thin films, grown using low-energy hydrocarbons. In this work, we investigate the reaction mechanisms of both the linear and the cyclic isomers of C_3 and C_3H on an *a*-C:H surface. We found that the cyclic species are always more reactive as compared to the linear species, due to their lower stability. The C_3 species are found to be more reactive than the C_3H species, due to steric hindrance of the H atom, shielding the C atom from the surface. The different mechanisms are discussed. The resulting film properties for different flux ratios of C_3 and C_3H have also been investigated. It is shown that films as deposited from C_3 and C_3H have a low density and show low cross-linking. A clear change in microstructure is observed as the ratio between the cyclic and the linear species changes. These simulations provide insights into the reaction behavior of the investigated species, and how this influences the resulting film properties. © *2006 American Institute of Physics*. [DOI: 10.1063/1.2150149]

I. INTRODUCTION

Since their preparation in the early 1970s,[1] diamondlike carbon (DLC) thin films have been studied extensively, both by experimental and computational means. The primary reason for this interest is their unique properties. DLCs occur in a wide variety of compositions, ranging from real diamondlike materials to glassy carbon structures and hydrogenated polymeric films.[2]

The diamondlike materials can be classified into two groups: "tetrahedral amorphous carbon," or ta-C, having a high hardness (>30 GPa), and *a*-C:H having a hardness in the range of 15–25 GPa. The ta-C films generally have a high hardness and Young's modulus, a low roughness, and a very low friction coefficient.[2,3] When hydrogen is incorporated into this type of film, tetrahedral hydrogenated amorphous carbon, or ta-C:H, is obtained. These films are used, for example, as wear-resistant coatings, on, e.g., magnetic hard disks and optical components. Experimentally, these materials are often fabricated using an ion source, producing high-energy carbon or hydrocarbon ions (~100 eV) bombarding the substrate. The high-energy ions can penetrate into the subsurface layers, causing a local increase in the density. The local bonding will then reform according to this new density, leading to a high sp^3 fraction.

The softer type of materials, which can be referred to as (hydrogenated) amorphous carbon, or *a*-C(:H), still exhibits a considerable hardness, with values of up to 25 GPa and even more, good adhesion, fracture toughness, and chemical stability[4,5] and can be used as, e.g., solid lubricants. This type of films can be produced[2] by, e.g., plasma-enhanced chemical-vapor deposition (PECVD). In contrast to the deposition of ta-C(:H), the ion flux fraction is lower than 100%, the exact value depending on the type of source used.[6] If high-energy ions are present, they can still contribute to the film growth by the same mechanism as for ta-C. However, in this case, also neutral species will contribute to the growth.

The contribution of the neutral species will depend on their individual sticking coefficients, which might depend on the ion flux. Diradicals can insert directly into surface C–C or C–H bonds, such that their sticking coefficient approaches 1. Monoradicals cannot insert directly into surface bonds but need a dangling bond at the surface. This dangling bond can be created by a removal of a hydrogen atom from a C–H surface bond either by ion displacement of H or by H abstraction.[7] Closed-shell neutrals show sticking coefficients close to zero, and their effect is negligible. In contrast to the subplantation mechanism in ta-C(:H) growth, which is a physical process, the deposition mechanism of *a*-C(:H) films occurs through a combination of physical subplantation and chemical surface reactions if ions are present or entirely through chemical reactions if no ions are present. Whether the subplantation mechanism will be operative under these conditions depends on the ion/radical flux ratio and the ion energy.

An efficient source to deposit *a*-C:H films is the so-called expanding thermal plasma[5,8] (ETP). In this type of

[a]Electronic mail: erik.neyts@ua.ac.be

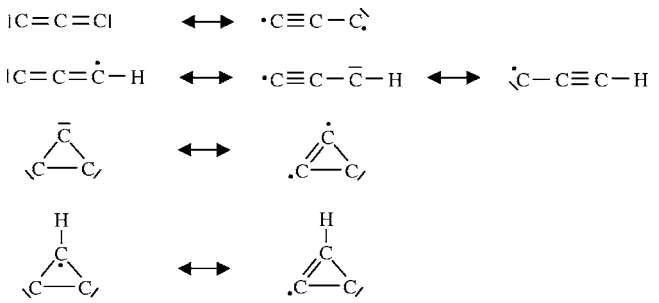

FIG. 1. Resonance structures of the isomers of the C_3 and C_3H radicals. All species except l-C_3H have resonance structures similar to the structures shown on the right sides of the arrows by symmetry.

source, no substrate bias has to be applied to obtain high-quality films,[9] with a hardness up to 14 GPa. Also, the deposition rate that can be achieved is very high, up to 70 nm/s, while preserving the quality of the films.[5,9] Most of the plasma chemistry and some of the particle-surface interactions have already been elucidated.[5,9] It was established that the major growth species depend on the ratio (F) between the C_2H_2 load and the Ar^+ and electron fluence emanating from the arc. At high C_2H_2 flows ($F>1$), it was established that C_3 and C_3H are the major growth species, using threshold ionization mass spectrometry[10] (TIMS). Deposition then occurs at a high rate, up to 70 nm/s, and films with a considerable hardness (14 GPa), refractive index (2.2), and low roughness (3.7 nm) are obtained.[5,8] However, it was not established which isomers of C_3 and C_3H are actually present in the plasma and/or deposit on the surface of the growing film.

For both species, two relatively stable isomers can be distinguished: the linear isomers, l-C_3 and l-C_3H, and the cyclic isomers, c-C_3 and c-C_3H (cf. Fig. 1). In the gas phase, these species are relatively unreactive.[11] At an a-C:H surface, however, they become very reactive, as will be shown later. Also, due to their totally different structure, they will exhibit different reaction mechanims with the surface. For example, the cyclic radicals are much less stable as compared to the linear species. Also, the carbon atoms in the cyclic radicals are more reactive than their counterparts in the linear species, due to their bonding configuration. Whether or not these radical-dependent factors and the corresponding reaction mechanisms codetermine the resulting film properties has not yet been investigated. Furthermore, the investigation of the reaction behavior of these species might also be important for other deposition techniques and in other fields, such as in interstellar space chemistry, since these species are relatively abundant in interstellar space.[12]

In this article, we have used molecular-dynamics (MD) simulations to elucidate the influence of the chemical structure of the different radical isomers on the resulting film structure, as well as their reaction mechanism with the a-C:H surface. Previously, we have already demonstrated that MD simulations can provide a tool to better understand the growth of this type of films under the ETP relevant conditions.[13]

The outline of the paper is as follows. In the following section, the MD simulation model is outlined. In Sec. III, we will present the results of the reaction characteristics of the different radical isomers. Finally, conclusions will be drawn in Sec. IV.

II. DESCRIPTION OF THE MODEL

The model used for this investigation was developed by Serikov *et al.*[14] and subsequently modified to increase the calculation speed. The interatomic potential used is the well-known Brenner potential for hydrocarbons.[15]

In the MD methodology, the atoms in the system are followed through space and time by integrating Newton laws. The atoms move under the influence of forces, taken as the negative of the analytical derivative of the interatomic potential. The integration scheme used is the velocity-Verlet algorithm.[16] Growth of the layers was obtained in the following manner. At first a substrate is defined. This initial substrate consists of 384 C atoms, forming a 2×1 reconstructed {111} diamond surface, equilibrated at 100 K. The bottom two atomic layers (128 atoms) are kept fixed to simulate a thick substrate and to anchor the simulation cell. Subsequently, a growth particle (l-C_3, c-C_3, l-C_3H, or c-C_3H) is selected and placed above the substrate, beyond the cutoff of the potential. The $\{x,y\}$ position of the growth particle is chosen on the basis of two random numbers. The rotational angles of the particle are also determined randomly. Each species is given a kinetic translational energy of 0.13 eV, and an internal energy of 0.026 eV, partitioned among the vibrational and rotational motions. A time step of 0.2 fs is applied for the integration, and each particle impact was followed for 2 ps. During this time, the particle can either stick on the surface, reflect from the surface, or abstract atoms from the surface. After 1.6 ps, a heat bath based on the algorithm of Berendsen *et al.*,[17] set at 100.0 K, was applied to dissipate the excess energy from the system. After 2 ps, atoms not bound to the substrate are removed, and a new impact is initiated on the resulting structure from the previous impact. After the films are deposited, they are analyzed as described below.

Five conditions have been investigated. These conditions are given in Table I, showing the growth species used to

TABLE I. Relative fluxes of the different growth species in the five films.

Film	Linear C_3	Linear C_3H	Cyclic C_3	Cyclic C_3H	Linear total	Cyclic total
Film 1	0.714	0.286	0.0	0.0	1.000	0.0
Film 2	0.714	0.143	0.0	0.143	0.857	0.143
Film 3	0.714	0.0	0.0	0.286	0.714	0.286
Film 4	0.357	0.143	0.357	0.143	0.500	0.500
Film 5	0.0	0.0	0.714	0.286	0.0	1.000

deposit the film and their relative fluxes. For every impact, the choice of the impinging particle is determined using a random number and based on these relative fluxes. The conditions were chosen specifically to test how the deposition and the resulting film change as the ratio between linear and cyclic growth species changes.

For the growth of the first film, simulated using l-C_3 and l-C_3H as the growth species, 2879 particle impacts were performed, which consist of 2065 l-C_3 and 814 l-C_3H impacts. Hence, this film is deposited using only linear species for the growth.

In the deposition of the second film, using l-C_3 and both the C_3H isomers, 2024 l-C_3, 410 l-C_3H, and 385 c-C_3H were used, adding up to 2819 impacts in total. This adds up to about 15% of cyclic particles contributing to the film growth.

For the third film, using l-C_3 and c-C_3H as growth species, 2331 impacts have been performed, which consist of 1636 l-C_3 and 695 c-C_3H impacts. For the growth of this film, the contribution of the cyclic species is now increased to about 30%.

In the fourth film, using both C_3 isomers and both C_3H isomers, 2256 impacts were performed in total which consist of 816 l-C_3, 320 l-C_3H, 804 $c-C_3$, and 316 c-C_3H impacts. Hence, about an equal amount of linear and cyclic species was used to deposit the film.

Finally, 1802 impacts were performed to simulate the fifth film, which consist of 1295 c-C_3 and 507 c-C_3H impacts. Hence, this film is entirely grown starting from cyclic particles.

The film deposited using l-C_3 and l-C_3H as growth species will be called "film 1;" hereafter, the film deposited using l-C_3 and c-C_3H will be called "film 2." Further, the simulated film using the l-C_3, l-C_3H, and c-C_3H growth species is called "film 3." The film simulated using l-C_3, c-C_3H, l-C_3H, and c-C_3H as growth species is called "film 4." The last film, deposited using c-C_3 and c-C_3H as growth species, will be called "film 5" hereafter. All films were grown until they reached a thickness around 18 nm.

From the numbers given above, it is already clear that the linear and the cyclic species have different sticking coefficients: almost 2900 impacts were needed to grow the first film, grown entirely from linear species and has a thickness of about 17 nm. On the other hand, only 1800 impacts were needed to grow the fifth film, which was grown starting from cyclic species only and has a thickness of about 19 nm. Below we will discuss the sticking probabilities in detail.

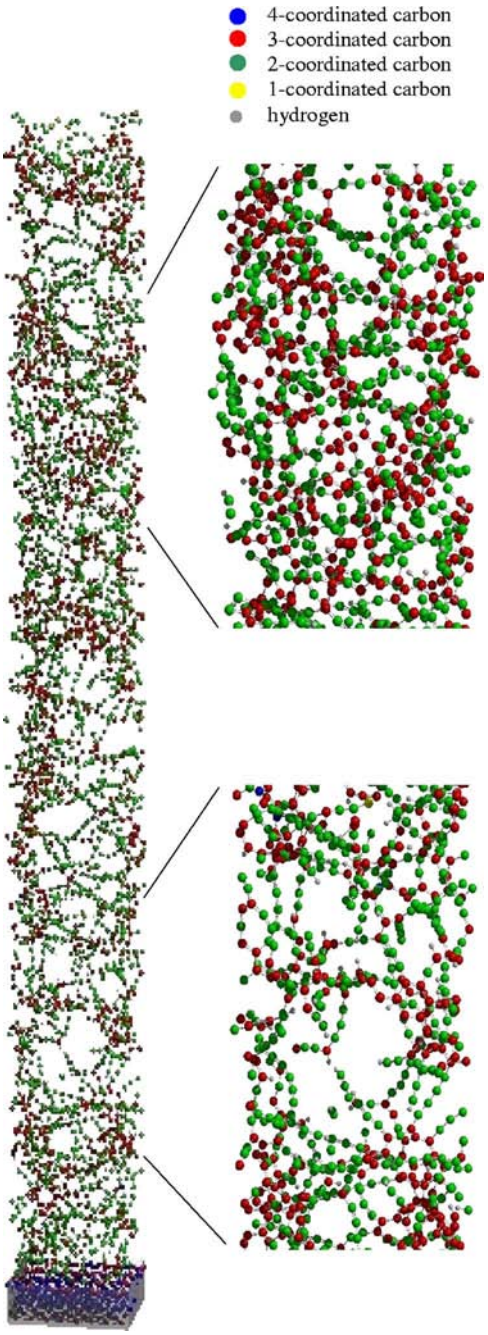

FIG. 2. (Color online) Calculated structure of film 1. The left-hand side shows the total structure. The right-hand side shows two regions in detail, showing different structural properties.

III. RESULTS AND DISCUSSION

A. Calculated film properties

In Fig. 2, the calculated structure of film 1 is shown as an example. The left-hand side of the picture depicts the structure as it is deposited in total; the right-hand side shows a more detailed view of two regions in the film. As can be seen, the film does not show much cross-linking (i.e., virtually no four-coordinated C atoms are present) but rather forms a chainlike network of sp- and sp^2-bonded carbon atoms, identifying one- and two-coordinated C atoms with sp carbons and three-coordinated C atoms with sp^2 carbons. This leads to porous structures. This is a general feature of the films deposited, which was observed in all five films grown (not shown). The microscopic details, however, depend on the applied conditions. While the overall structure of all five films is similar, they differ from each other in their microscopic structure. For example, in the first film, it can be seen from the detailed pictures (right-hand side) that there are several transitions visible in the structure; very close to the substrate, a relatively dense structure is formed, followed by a region of very low density. Finally, the "equilibrium" structure is formed, showing a higher density. It should be emphasized that these structures are formed keeping the deposition conditions (temperature, species, species fluxes,

TABLE II. Average density, C-coordination number Z_C, and the sp^1 and sp^2 carbon fractions as calculated in the different films.

Film	Rho (g cm^{-3})	Z_C	sp^1	sp^2
Film 1	1.14	2.43	0.57	0.43
Film 2	1.15	2.52	0.48	0.52
Film 3	1.22	2.59	0.41	0.59
Film 4	1.13	2.59	0.41	0.59
Film 5	1.10	2.57	0.42	0.58

etc.) constant. Although different from one another, similar transitions are also observed in the other films.

Averaged over the bulk region of the films, the calculated density of the films is between 1.1 and 1.2 g cm^{-3} (cf. Table II). A maximum film density is observed in the third film, which was grown using a ratio of about 70/30 between the linear and the cyclic radicals. Experimentally,[10] the density was found to be in the range of 1.5–1.7 g cm^{-3}. However, the hydrogen content in the experimentally deposited films is about 30%, which can only be accounted for if an additional H flux towards the substrate is present. Preliminary MD simulations have shown that an additional H flux could increase the density. In the future work, the effect of this additional H flux will be thoroughly investigated. In the films deposited in this work, the H content is about 8%. During the radical impacts, no H atoms are eliminated from the surface. Hence, the stoichiometry of the film is entirely due to the stoichiometry within the particle fluxes.

The general structure of the films is further characterized by the coordination numbers of the carbon atoms. The average carbon coordination numbers Z_C and the sp^1 and sp^2 carbon fractions are given in Table II. Z_C as a function of film thickness is shown in Fig. 3. It is clear from the table that the predicted structures are entirely composed of two- and (especially) three-coordinated C atoms. Both Table II and Fig. 3 show that the C-coordination number is the lowest in film 1, in agreement with the low density, increases as the fraction of cyclic species increases, and reaches a plateau when the flux of the cyclic species is about 30% of the total species flux towards the substrate.

Besides the C-coordination numbers, it is interesting to consider the distribution of C–C coordinations. For example, if a hard film is desired, one would try not only to maximize the sp^3 fraction in the film but, more importantly, to increase the fraction of sp^3 C atoms bonded to other sp^3 C atoms. In Fig. 4, the C–C coordination is shown for the five films. It can be seen in Fig. 4 that there is a clear shift in their bond distributions. The fraction of 2-2 C–C bonds (i.e., the fraction of C–C bonds that connect a two-coordinated carbon atom to another two-coordinated carbon atom) decreases as the fraction of cyclic species sticking to the surface increases, corresponding to an increase in the fraction of 3-3 C–C bonds. This is directly related to the sticking mechanism of the different isomers, as will be explained in Sec. III B.

Figure 5 presents the calculated fractions of C–C bond energies, relative to the total number of C–C bonds. Note that the single C–C bond as in ethane has a bond strength of about 3.6 eV, a double C–C bond as in ethene 6.4 eV, a triple C–C bond as in ethyne 8.7 eV, a conjugated C–C bond as in benzene 5.2 eV, and a C–H bond as in methane about 4.3 eV.

All films contain virtually only two- and three-coordinated C atoms, and there are practically no C–C bonds stronger than 6.5 eV. Hence, triple bonds are entirely absent in all films. It is also clear from the figure that as the fraction of deposited linear species decreases, the fraction of "true" double C–C bonds decreases. While this fraction is about 0.32 in film 1 (deposited using only linear species), it is only about 0.12 in film 5 (deposited using only cyclic species). These double bonds can be attributed almost exclusively to two-coordinated C atoms. Although a three-coordinated C atom also forms either one double bond and two single

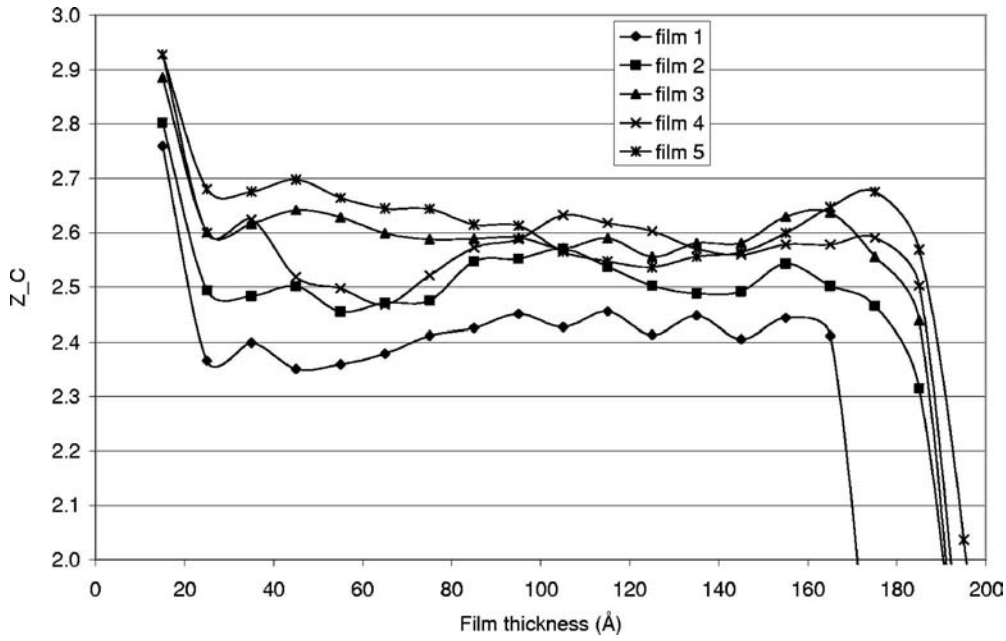

FIG. 3. Average carbon coordination number Z_C as a function of the film thickness.

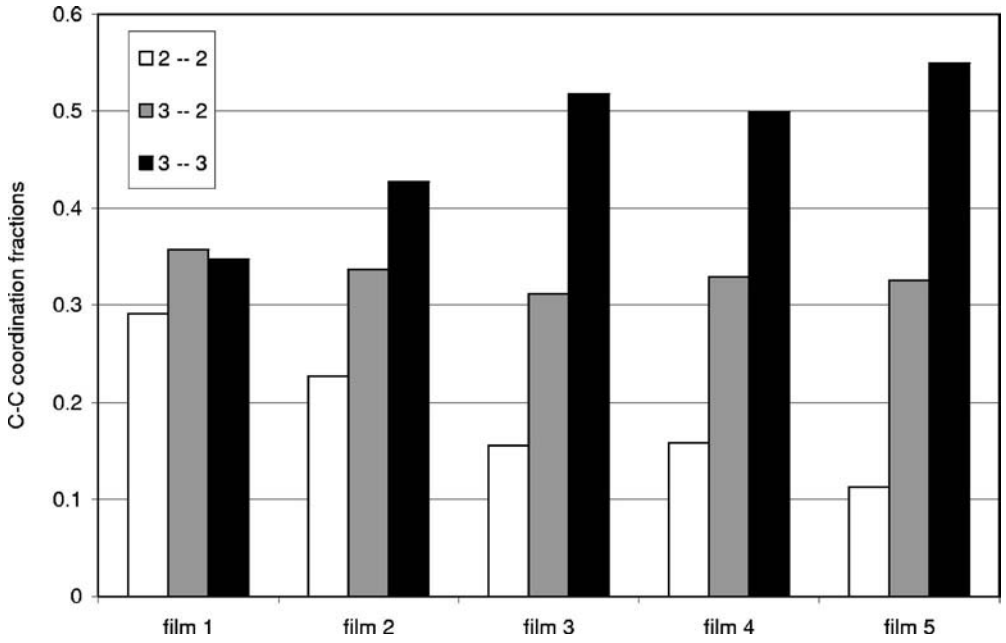

FIG. 4. Calculated histogram showing the C–C coordination numbers in the five films.

bonds or two double bonds, these bonds are conjugated, which explains the increasing fraction of bonds around 5.0 eV as the fraction of sticking cyclic species increases. Moreover, the fraction of single bonds, with an energy of about 3.5 eV, is negligible. Hence, it can be concluded that the three-coordinated C atoms form three similar bonds, resulting in a kind of polymeric structure.

B. Deposition characteristics of the *l*-C_3, *c*-C_3, *l*-C_3H, and *c*-C_3H radicals

From the short analysis of the films given above, it becomes clear that the films are not very different from each other with respect to their general structure (i.e., comparable density and coordination fractions), but they do differ with respect to their microscopic structure (i.e., the C–C coordination distribution). Both the similarities and the differences can be explained by considering the actual growth of the film and, in particular, the role of the reaction mechanisms of the different isomers with the structures formed.

1. The linear C_3 and C_3H radicals

The *l*-C_3 radical is a depositing species in films 1–4. It has a moderate sticking coefficient between 0.4 and 0.5. The *l*-C_3H species deposits in films 1, 2, and 4 and has a sticking coefficient between 0.3 and 0.4. The calculated values for the different films are given in Table III. From this table, it is

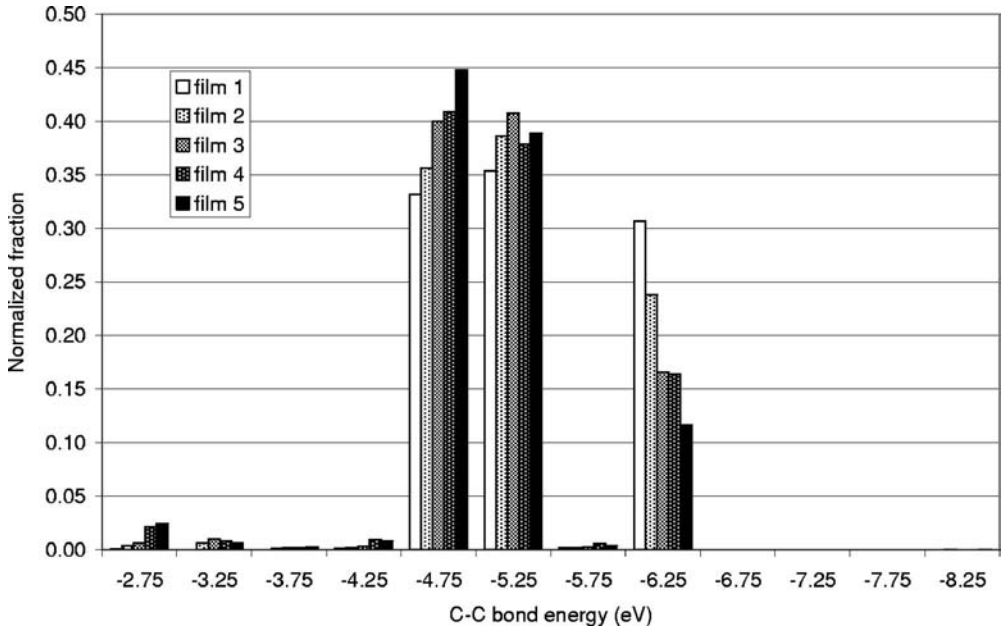

FIG. 5. Calculated histogram showing the energy distribution of the C–C bonds in the five structures.

TABLE III. Calculated sticking coefficients of the different growth species in the different films.

Film	Linear C_3	Linear C_3H	Cyclic C_3	Cyclic C_3H
Film 1	0.42	0.33	···	···
Film 2	0.43	0.36	···	0.56
Film 3	0.49	···	···	0.68
Film 4	0.52	0.38	0.66	0.62
Film 5	···	···	0.74	0.67

clear that their reactivity increases as the fraction of depositing cyclic species increases, as is especially clear for the C_3 radical. Moreover, when the fraction of depositing cyclic species increases, the *l*-C_3 radical sticks more with two atoms instead of one, indicative of a more reactive surface. In about 85% of its sticking events, it sticks with one of the outer carbon atoms and in about 13% of the events with both of the outer carbon atoms. The middle carbon atom is fully bound, inducing repulsive forces between this atom and the surface during impact. Hence, the middle carbon atom is virtually never involved in bonding to the surface.[18] The outer carbon atoms on the other hand have electrons not participating in the interatomic bonds in the gas phase, such that these are available for bonding to the surface. The average sticking energy for the C_3 radical is −5.29 eV when it sticks with one atom and −9.96 eV when it sticks with both outer carbon atoms.

The situation is somewhat different for the *l*-C_3H radical. While the *l*-C_3 radical has two equivalent carbon atoms available for binding to the surface, one of the outer C_3H radical carbon atoms is shielded by the H atom, leaving only one carbon atom readily available for binding to the surface. This explains its lower reactivity as compared to the C_3 radical. On average, its sticking energy is −5.21 eV.

When the *l*-C_3 radical sticks to the surface with one of its outer carbon atoms, the interatomic bond connecting the middle carbon atom and the surface binding atom becomes stronger with on average about 1.2%. The other bond, connecting the middle carbon atom and the atom that is not connected to the surface, becomes weaker with about 1.4%. When both outer carbon atoms are binding to the surface, both the intramolecular bonds become stronger, although only by about 0.5% or less. An example of the evolution as a function of time of the different *l*-C_3H bonds is shown in Fig. 6.

In the case of the *l*-C_3H radical, the interatomic bond between the binding atom (almost invariably the outer, nonhydrogen-carrying C atom) and the central C atom becomes stronger with a value between 0.7% and 1.3%, increasing as the fraction of cyclic depositing species increases. The other interatomic C–C bond becomes weaker with more than 1.6%.

If the C_3 radical sticks to the surface, the sticking atom becomes two coordinated. Hence, irrespective of how the radical sticks to the surface, the radical atoms do not become three coordinated upon impact. Obviously, they can become three coordinated as a result of later impacts. While the H-carrying C atom in the C_3H radical could become three coordinated if it would bind to the surface, this mechanism almost never occurs, such that also the C_3H radical does not promote the *sp* to sp^2 shift of one of its atoms. This explains the chainlike structures of films 1 and 2. (In film 2, only a fraction of 0.143 of the impacting species has a cyclic structure.)

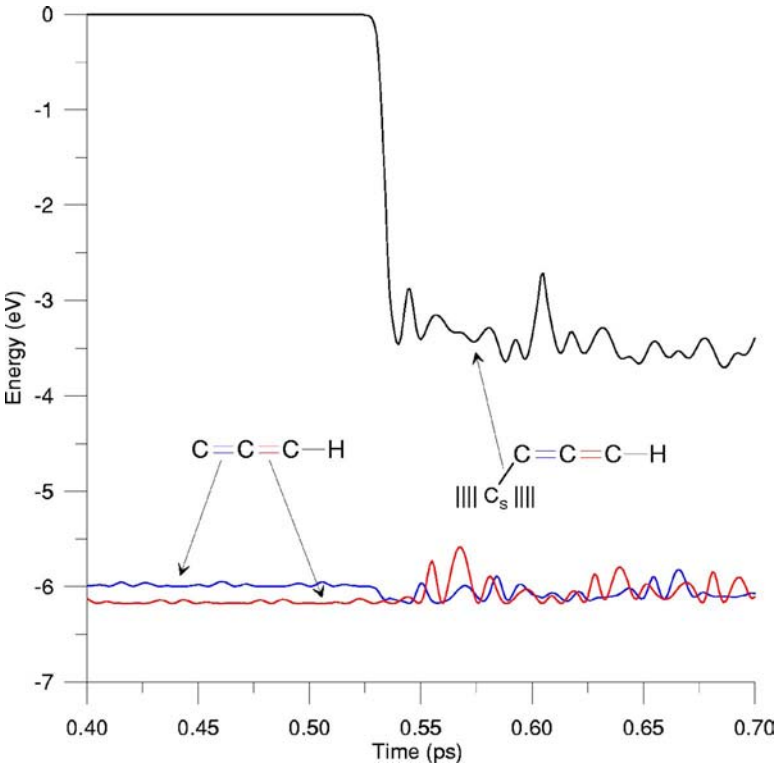

FIG. 6. (Color online) Time evolution of the bond energies in the C_3H radical upon impact and sticking on the surface.

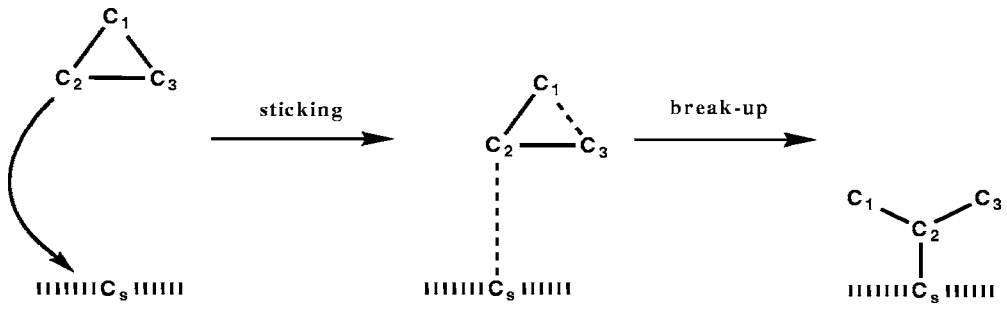

FIG. 7. Schematic representation of the sticking and breaking up of an impacting cyclic C_3 radical. In this illustration, the C_1–C_3 bond breaks up, but obviously the C_1–C_2 or C_2–C_3 bonds can also break up upon impact.

2. The cyclic C_3 and C_3H radicals

While the analysis of the impact behavior of the linear isomers is relatively straightforward, the cyclic isomers show a more complex behavior. Nevertheless, several general trends can be observed.

First of all, it should be pointed out that the cyclic radicals are structurally unstable. The ring strain in the cyclopropane molecule (cyclic C_3H_6), for example, is about 1.2 eV, lowering the bond strengths with about 32% as compared to the linear propane molecule. In c-C_3 and c-C_3H the bond strengths are lowered even more by about 50% relative to the bonds in the linear isomers. Second, each carbon atom in the cyclic radicals has at least one electron available to share in chemical binding to the surface, contrary to the linear isomers. Hence, it is predicted that the reactivity of the cyclic isomers should be higher than the reactivity of the linear radicals. This is indeed substantiated by our simulations, as can be seen in Table III. Further, the reactivity of c-C_3 should be higher than that of c-C_3H, since the H atom on c-C_3H partially shields one carbon atom from binding to the surface. This effect is also seen in the simulations.

The cyclic C_3 radical is a growth species in films 4 and 5, showing a sticking coefficient of 0.67 and 0.74, respectively. In more than 70% of its sticking events, it sticks with one atom, to be compared with the value of 85% for the linear isomer. In the remaining 30% of its sticking events, the c-C_3 radical sticks with two atoms to the surface. This is a consequence of the fact that all of its carbon atoms are available for binding to the surface, contrary to the linear C_3 species. Hence, the reactivity and sticking behavior of the cyclic radical is unaffected by the exact orientation of the radical relative to the surface, which is not the case for the linear isomer. When the c-C_3 radical sticks to the surface with one atom, the sticking energy is on average −5.37 eV; when two bonds to the surface are formed, the average sticking energy is −10.18 eV.

Upon impact, the c-C_3 molecule easily breaks up; in about 70% of its sticking events, the molecule first binds to the surface, immediately followed by breaking of one of the intramolecular bonds. An example of this process is shown schematically in Fig. 7. The figure shows that the c-C_3 radical can, in fact, become three coordinated upon impact, contrary to the *linear* isomer. Cyclic radicals that remain intact upon impact can break up due to later impacts as well. Only a small fraction ($<5\%$) will remain intact. As mentioned above, the driving force for this breakup is the ring strain in this radical. When an intramolecular bond is broken, the ring strain is relieved, and a linear species is formed. Hence, the interatomic bond strengths in the radical are strongly increased, comparable to the bond strengths in the linear radicals (~5 eV). As a result, the single bonds of the gas phase cyclic radicals are converted into double bonds, leading to the bond energy histogram, as shown in Fig. 5.

As mentioned above, the linear C_3 radicals almost invariably stick with one of the outer carbon atoms, leading to two-coordinated surface binding radical atoms upon impact. In contrast, in the case of a cyclic C_3 radical, the surface binding radical atom becomes three coordinated in more than 40% of the sticking events. This effect promotes the sp to sp^2 shift of one of the atoms of the impacting c-C_3 radical. It can be concluded that this effect, together with the enhanced reactivity, induces the higher sp^2 fraction in the films deposited partially from cyclic radicals, as compared to the films deposited by mainly linear species.

The c-C_3H radical deposits in films 2–5. The general picture for c-C_3 remains largely unchanged when considering the c-C_3H radical. That is, a severe ring strain is present in the molecule, causing the molecule to easily break up upon impact, and the absence of a fully bonded C atom that would induce repulsive forces. Both factors enhance its reactivity as compared to the l-C_3H radical. Similar to the effect of the H atom in l-C_3H radical, the H atom in c-C_3H radical partially shields the carbon atom attached to it from the surface. Hence, most sticking events happen with one of the non-H-carrying C atoms (>80% in films 2 and 4). In film 3, this percentage of sticking with one atom is reduced to 77% and in film 5 to 74%. Similar to the c-C_3 radical, the remaining of its sticking events involves the formation of two bonds, connecting two radical atoms to the surface. Sticking to the surface with one atom involves an energy of −5.30 and −9.88 eV when sticking with two atoms.

The break-up mechanism occurs in only about 60% of its sticking events in films 2 and 4, to be compared with 70% for the c-C_3 radical. In the third film, the c-C_3H radical breaks up in 64% of its sticking events and in 73% in the fifth film. Hence, except for the fifth film, the break-up percentage of c-C_3H radical is reduced by 5%–10% as compared to the c-C_3 radical.

IV. CONCLUSION

Molecular-dynamics simulations have been performed to investigate the sticking behavior and the reaction mechanisms of the linear and cyclic isomers of C_3 and C_3H species.

We have investigated how the different structure of the C_3 and C_3H species results in different sticking mechanisms on an *a*-C:H surface. We have shown that (1) the cyclic species are always more reactive as compared to the linear species, resulting in higher sticking coefficients; (2) the cyclic species always have one reactive carbon atom more than their linear counterparts, due to their bonding configuration; and (3) the cyclic species are geometrically less stable than the linear species. This results in the cyclic radicals frequently breaking up, enhancing their reactivity; and (4) the C_3 radicals are more reactive than the C_3H radicals, due to steric hindrance of the H atom, shielding the C atom from the surface.

The resulting film properties for different flux ratios of cyclic C_3 and C_3H have also been investigated. It is shown that the deposited films have a low density and show low cross-linking. When predominantly linear growth species are used, a more chainlike structure evolves. Increasing the percentage of cyclic species impacting and sticking on the surface, the fraction of three-coordinated C atoms increases, at the expense of the two-coordinated fraction. A maximum film density is obtained using a 70/30 mixture of linear and cyclic radicals.

Finally, under the growth conditions used, i.e., only C_3 and C_3H contribute to growth, it has also been shown that the H elimination through incoming radicals does not occur; hence, the stoichiometry of the films is determined entirely through the stoichiometry of the sticking species.

These results have important implications to understand thin *a*-C:H film growth from (at least partially) low-energy hydrocarbons, as is, e.g., the case in an Ar/C_2H_2 expanding thermal plasma. Furthermore, the results provide important values for sticking probabilities, which are needed for plasma simulations.

ACKNOWLEDGMENTS

One of the authors (E.N.) is indebted to the Institute for the Promotion of Innovation by Science and Technology in Flanders (IWT-Flanders) for financial support. The authors would like to thank J. Benedikt for the many fruitful discussions on the chemistry in the ETP plasma and the deposition mechanisms and also Professor R. Gijbels for the interesting discussions.

[1] S. Aisenberg and R. Chabot, J. Appl. Phys. **42**, 2953 (1971).
[2] J. Robertson, Mater. Sci. Eng., R. **37**, 129 (2002).
[3] J. Robertson, J. Non-Cryst. Solids **299–302**, 798 (2002).
[4] http://www.bekaert.com/bac/products/diamond-like%20coatings.htm
[5] J. Benedikt, M. Wisse, R. V. Woen, R. Engeln, and M. C. M. van de Sanden, J. Appl. Phys. **94**, 6932 (2003).
[6] J. Robertson, in *Diamond and Diamondlike Films and Coatings*, NATO Advanced Studies Institute, Series B: Physics, edited by J. C. Angus, L. L. Horton, and E. R. Clausing (Plenum, New York, 1991), Vol. 266, p. 243.
[7] M. Meier and A. von Keudell, J. Appl. Phys. **90**, 3585 (2001).
[8] J. W. A. M. Gielen, M. C. M. van de Sanden, P. R. M. Kleuskens, and D. C. Schram, Plasma Sources Sci. Technol. **5**, 492 (1996).
[9] J. Benedikt, D. J. Eijkman, W. Vandamme, S. Agarwal, and M. C. M. van de Sanden, Chem. Phys. Lett. **402**, 37 (2005).
[10] J. Benedikt, S. Agarwal, D. Eijkman, W. Vandamme, M. Creatore, and M. C. M. van de Sanden, J. Vac. Sci. Technol. A **23**, 1400 (2005).
[11] H. H. Nelson, H. Helvajian, L. Pasternack, and J. R. McDonald, Chem. Phys. **73**, 431 (1982).
[12] H. Yamagishi, H. Taiko, S. Shimogawara, A. Murakami, T. Noro, and K. Tanaka, Chem. Phys. Lett. **250**, 165 (1996).
[13] E. Neyts, A. Bogaerts, R. Gijbels, J. Benedikt, and M. C. M. van de Sanden, Diamond Relat. Mater. **13**, 1873 (2004).
[14] V. V. Serikov, S. Kawamoto, C. F. Abrams, and D. B. Graves, APS Proceedings of the 22nd Symposium on Rarefield Gas Dynamics, Sydney, 2000 (unpublished).
[15] D. W. Brenner, Phys. Rev. B **42**, 9458 (1990).
[16] W. C. Swope, H. C. Anderson, P. H. Berens, and K. R. Wilson, J. Chem. Phys. **76**, 637 (1982).
[17] H. J. C. Berendsen, J. P. M. Postma, W. F. van Gunsteren, A. DiNola, and J. R. Haak, J. Chem. Phys. **81**, 3684 (1984).
[18] D. N. Ruzic and D. A. Alman, Presented at the Tenth International Workshop on Carbon Materials for Fusion Application, Jülich, Germany, 17–19 September 2003 (unpublished).